CORROSION SCIENCE AND TECHNOLOGY, Vol.6, No.4(2007), pp.147~153

Effects of W Contents in Co Matrix of the Thermal Sprayed WC-Co on the Corrosion Behavior in Molten Zinc

Byeong-Geun Seong[1], Sun-Young Hwang[1], Kyoo-Young Kim[2], and Kee-Ahn Lee[3,†]

[1]*New Metals Research Department, RIST, Pohang, Kyungbuk, 790-330, Korea*
[2]*Graduate Institute of Ferrous Technology, POSTECH, Pohang, 790-784, Korea*
[3]*School of Advanced Materials Engineering, Andong National University, Andong, 760-749, Korea*

This study sought to investigate the reaction of Co-binder containing tungsten with molten zinc. Four kinds of Co-W alloys (pure, 10%W, 20%W, 30%W) were prepared using the powder metallurgy method. The specimens were immersion-tested in molten pure zinc baths at 460 ℃. To evaluate the corrosion property in molten zinc, the weight loss of the specimen was measured after the immersion tests at different immersion times (10~300 min.). Co-10%W alloys, compared with pure cobalt, showed no effect of tungsten addition on the reaction rate in molten zinc. The relationship between the weight loss and the square root of immersion period represents a straight line in both pure cobalt and Co-10%W alloy. The Co-Zn reaction layer in Co-10%W alloy consists of $\gamma 2$, $\gamma 1$, γ and $\beta 1$ phases. The rate of weight loss significantly increases and the weight loss behavior is not well accord with the linear relationship as the tungsten content in the Co-W alloy increases. The $\beta 1$ layer was not formed on the Co-20%W alloy and neither was a stable Co-Zn intermetallic compound layer found on the Co-30%W alloy. The main cause of increase in reaction rate with increasing tungsten content is related with the instability of the Co-Zn reaction phases as seen on micro-structural analysis.

Keywords *: WC-Co coating, Co-binder containing tungsten, thermal spray, immersion test in molten zinc, $\beta 1$ phase, $\gamma 2$ phase*

1. Introduction

Recently, the continuous galvanizing process is experiencing resurging demand because of greater need for galvanized steel sheets for production of automobiles, buildings, and home electric applications. In a continuous galvanizing line (CGL), pot roll surface conditions are very important because they are in direct contact with the steel sheets in the zinc pot. Stainless steels are generally used as roll materials, but their corrosion resistance to molten zinc is not good.[1)] Thus, zinc pot rolls are commonly coated with WC-Co to protect the pot roll surface from severe corrosion by molten zinc.[2)-4)]

Although there are many reports on the reaction between the molten zinc and ferrous materials,[5)-7)] only a limited amount of research has been performed on the reaction between the molten zinc and WC-Co coating materials.[8),9)] In a previous paper, the authors found that the WC-Co coating layer was usually composed of three binding phases, i.e. WC, Co_3W_3C, and Co.[10),11)] The Co binder was suggested as the most important phase among those three for the reaction behavior between WC-Co coating and molten zinc.[10),11)] Furthermore, it is very difficult to analyze the WC-Co coating samples that have reacted with molten zinc and to understand the exact reaction mechanism because of the indistinguishable microstructure. Consequently, the reaction behavior of pure Co phase in the WC-Co coating with molten zinc has been investigated.[12)] However, it has been also reported that the Co-binder may not be pure and can easily contain an amount of tungsten as a solid solution.[13)] It is thus the purpose of this study to investigate the reaction behavior of the Co phase containing tungsten with molten zinc and to discuss the mechanism for the corrosion of WC-Co coating.

2. Experimental

According to the Co-W binary phase diagram,[14)] the maximum solubility of tungsten in Cobalt has been known as 39.8 wt.% especially at 1471℃. In the thermal spray coating process, a rapid cooling rate of approximately 10^6

† Corresponding author: keeahn@andong.ac.kr

℃/s after heating above 1600℃ can induce higher tungsten solubility than that of equilibrium in the phase diagram. Thus the compositions of Co-W alloys were chosen as Co-10%W, Co-20%W and Co-30%W. Specimens were prepared by powder consolidation method. The particle sizes of Co and W powders were 0.36~0.96 μm and 0.88 μm, respectively. Co-W powders were mixed as 9 : 1, 8 : 2 and 7 : 3 wt.% ratio and ball milled using a super-hard ball for 10 hours. The powder mixture was separately weighed into 15 g units and placed into a mold of 16 mm ϕ and pressed with 5 tons of pressure into a cylindrical shape. Vacuum sintering process was also performed. The cylindrical specimen was heated at a 10℃ /min rate to 1400℃, maintained for 2 hours, and subsequently furnace-cooled. Each sample was glass sealed again and solution heat treated at 1250℃ for 30 minutes, and then directly water quenched after breaking the sealing. The specimen dimensions for the molten zinc immersion test were 8 mm×12 mm×2 mm. The specimen received a 2 mm hole punched into one end and was hung by tungsten wire in the molten zinc. Tungsten is generally known as being non reactive to zinc. The immersion tests in the molten pure zinc bath (99.99%, 8~9 kg) were carried out at 460℃ under a N_2 environment. To evaluate the degradation properties, the weight loss of the Co specimen was measured after the immersion test at different immersion times – 10, 30, 60, and 300 minutes. For observation of the Co-Zn compound layers on the surface, immersed specimens were analyzed with optical microscope (OM), scanning electron microscope (SEM), and energy dispersive spectrum (EDS).

3. Results

Fig. 1 shows the XRD patterns of Co-10%W, Co-20%W and Co-30%W specimens to confirm the complete solid solution of tungsten element in the Cobalt matrix. Co_3W precipitation can be expected to appear in the case of an incomplete solid solution. It is clear in this figure that the prepared samples didn't contain the Co_3W phase. The specimens were analyzed and found to consist mainly of the Co phase. However, unexpected $CoWO_4$ oxides were also detected in the X-ray diffraction patterns. Though the $CoWO_4$ phase is rarely observed in the Co-10%W specimen, the peaks of $CoWO_4$ change to be comparatively apparent with increasing tungsten content (Co-20%W and Co-30%W specimens). Oxides are thought to be formed due to the air voids in a consolidated specimen, which can't escape during the vacuum sintering process.

Fig. 2 shows the weight loss per unit area vs. the square root of immersion period (t) results for Co-10%W, Co-20%W and Co-30%W alloys immersed in pure zinc at 460℃. Co-10%W alloy represents a weight loss behavior similar to that of pure cobalt. As the tungsten content in the cobalt increases up to 20% or 30%, the amount of weight loss becomes significantly larger. It is also important that the weight loss of Co-10%W alloy linearly

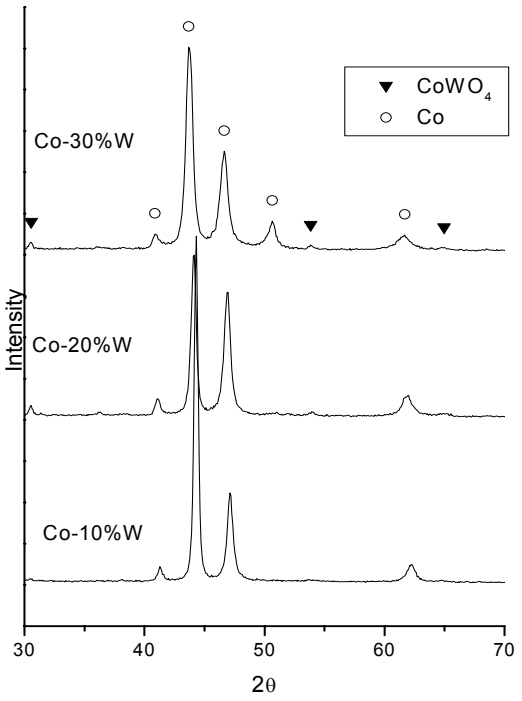

Fig. 1. X-ray diffraction patterns for the Co-10%W, Co-20%W, Co-30%W alloy specimens after sintering, solutionizing, and water quenching.

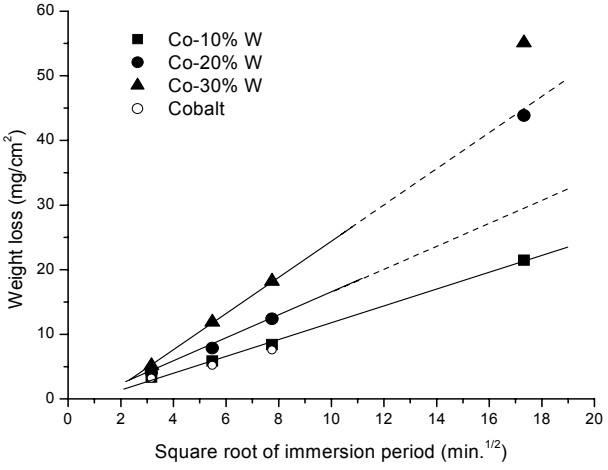

Fig. 2. Weight loss vs. square root of immersion time for Co-10%W, Co-20%W and Co-30%W alloys immersed in pure zinc at 460℃.

increased with an increase in the square root of time, closely matching the parabolic rate rule. A previous study for the reaction of pure cobalt with molten zinc has similarly reported that the relationship between weight loss after the immersion test and immersion time follows the typical parabolic rate law.[12] On the other hand, the weight loss behaviors of both Co-20%W and Co-30%W alloys do not fall within the linear relationship mentioned above and the amount of weight loss increases remarkably more than expected, especially with an immersion time of 5 hours.

Fig. 3 shows the optical micrographs of the reacted layers in molten zinc at 460℃ for 30 min. In the case of the Co-10%W alloy (Fig. 3 (a)), a Co-Zn compound is formed between the Zn and Co-W alloy and observed as a white layer with inhomogeneous thickness. The Co-Zn compound of Co-20%W alloy represents an irregular layer with a blooming burst characteristic. In the case of 10-30%W alloy, on the contrary, there is an absence of a continuous layer of Co-Zn compound along the interface. Instead, small, white particles are distributed in the black Zn layer (Fig. 3 (c)).

In previous results,[12] four kinds of Co-Zn intermetallic compound layers, $\beta 1$, γ, $\gamma 1$ and $\gamma 2$ could be divided after immersion of pure cobalt in a molten zinc bath and confirmed by both microstructural observation and electrochemical stripping method. Fig. 4 shows the SEM back-scattered images of Co-10%W and Co-20%W specimens that reacted with zinc at 460℃ for 60 min. The chemical compositions of point A, B, C, D, E, F, and G in the figure were also analyzed by EDS. It is somewhat difficult to divide each reaction phase in the image of Co-Zn compound layer (Fig. 4) and unlikely in the case of pure cobalt.[12] However, a thin Co-Zn compound layer (written as A) can be observed in Fig. 4 (a) between the bright Co-Zn compound layer and the dark cobalt matrix. The atomic composition ratio of this layer (A) is almost 1 : 1 for Co : Zn. Considering both the chemical analysis result and the cobalt-zinc binary phase diagram,[15] this thin Co-Zn compound layer of Co-10%W alloy can be reasonably determined as $\beta 1$ phase. This $\beta 1$ layer represents unstable characteristics reflected in the disappearance of the discontinuous layer, especially around the region on the left in Fig. 4 (a). It is also found in this figure that the zinc contents of points B, C, and D increase gradually with moving analysis area to Zinc. Comparing the theoretical composition in Co-Zn binary diagram[15] with the

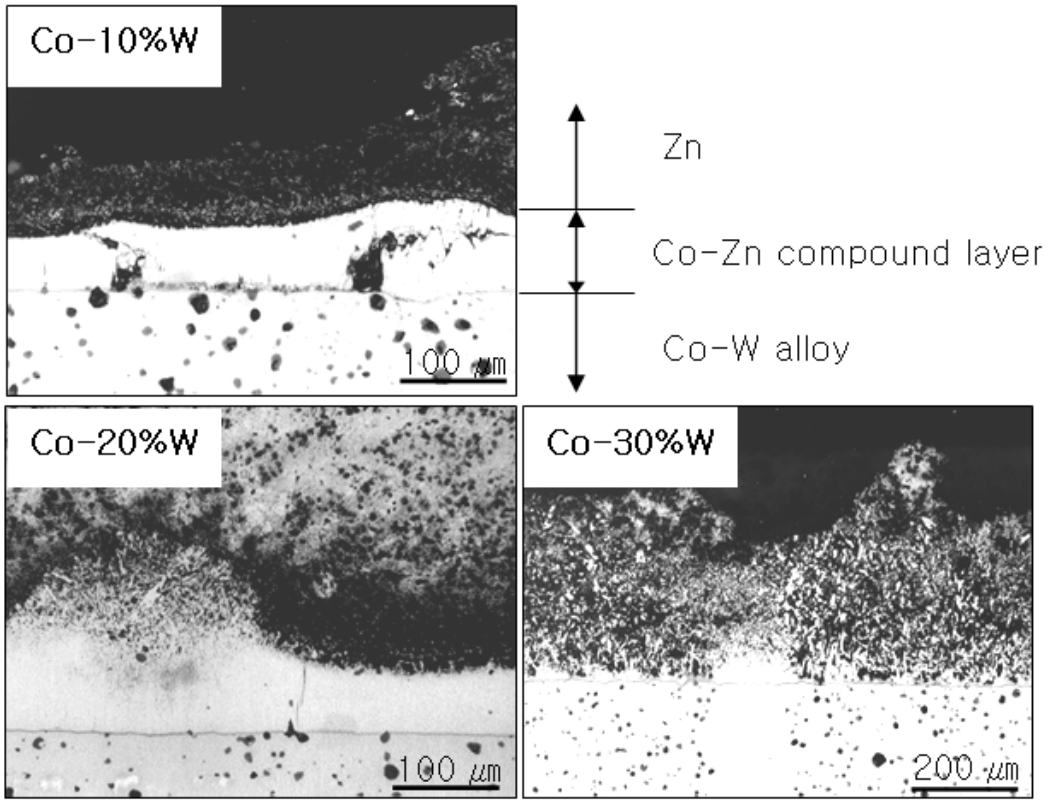

Fig. 3. Cross-sectional optical micrographs of Co-W alloys after reaction with molten pure zinc at 460℃ for 30 min.

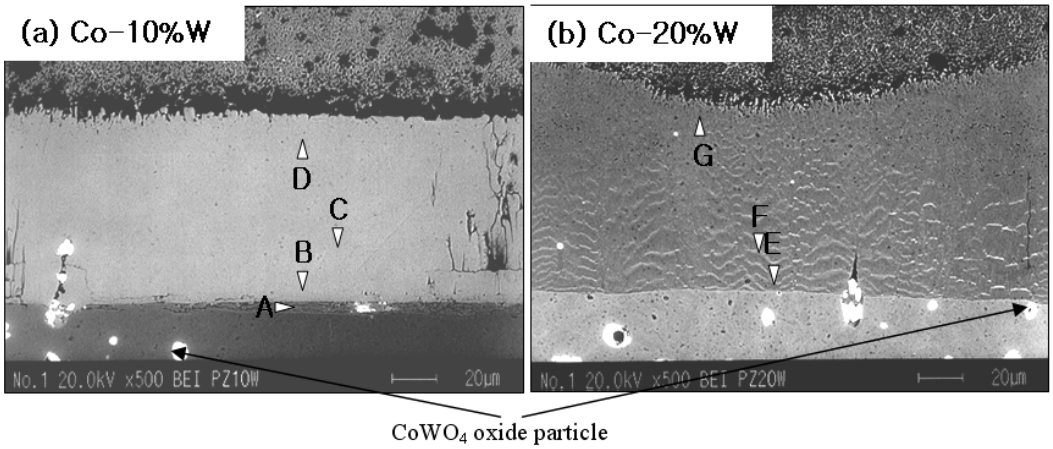

Position	Co (at.%)	W (at.%)	Zn (at.%)
A	46.40	0.96	52.64
B	18.40	-	81.60
C	11.24	-	88.76
D	7.34	-	92.66
E	16.14	1.73	82.13
F	9.88	2.62	87.50
G	7.06	1.06	91.88

Fig. 4. BEIs and chemical compositions analyzed by EDS for the Co-10%W and Co-20%W alloys after immersion in a pure zinc at 460℃ for 60 min.

above experimental results, it can be generally assumed that points B, C, and D correspond with γ, $\gamma 1$ and $\gamma 2$ phases. These three phases are difficult to distinguish and seem to be continuously mixed as a composite layer. From the above results, it can be induced that the Co-Zn reaction layer in Co-10%W alloy consists of four compound phases-- $\gamma 2$, $\gamma 1$, γ and $\beta 1$, similar with those in pure cobalt.

In the case of Co-20%W alloy (Fig. 4 (b)), it is inferred from the chemical composition results of three different areas (E, F, and G) that the Co-Zn reaction layer mainly consists of three compound phases-- $\gamma 2$, $\gamma 1$ and γ. The $\beta 1$ layer cannot be found in this alloy. Many white wavy patterns in the layer are noted in this figure. Composition analysis also indicates that the wavy patterns contain significantly higher W contents than the Co-Zn compound layer. Similar features of concentration of a non-reactive element have also been reported in the reactions of the WC-Co consolidated specimen[16] and Co_2Si specimen[17] with molten Zinc.

Fig. 5 shows the SEM back-scattered image and chemical compositions analyzed by EDS for the Co-30%W specimen. It is apparently found that only $\gamma 2$ phases (J) are mixed and distributed in the Zinc matrix (K) instead of composing a stable layer of Co-Zn compound. Oxide

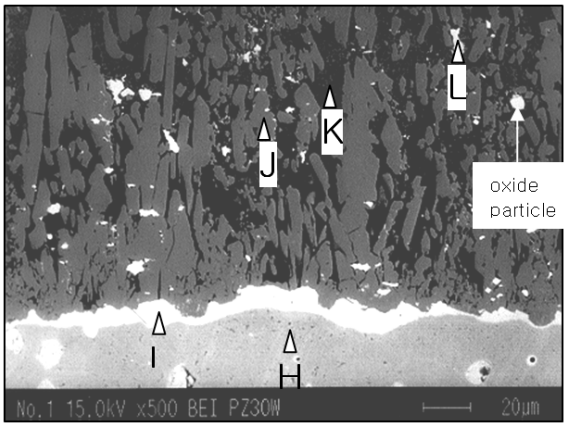

Position	Co (at.%)	W (at.%)	Zn (at.%)
H	85.85	14.15	-
I	4.49	17.76	77.75
J	6.56	-	93.44
K	0.66	-	99.34
L	1.41	16.72	81.86

Fig. 5. BEI and chemical compositions analyzed by EDS for the Co-30%W alloy after immersion in a pure zinc bath at 460℃ for 60 min.

particles with round shape and white tungsten-rich particles (L) are distributed separately throughout the mixture

in the $\gamma 2$ phase and Zinc matrix. A white tungsten-rich layer (I, Zn-W-Co layer) is also observed on the surface of the Co base metal. The phase (I) seems to be unstable judging from the inconsistent layer thickness. Previous studies have reported that a compound cannot be formed in Zn-W binary system.[18),19)] Thus, it is assumed in this study that cobalt can play a role as the bonding intermediate for the formation of the Zn-W compound. Because the Zn-W-Co layer is so unstable, the Co-Zn compound can be easily separated from the surface of the layer and distributed in the zinc matrix. The significant weight loss in Co-30%W, which is seen in Fig. 2, is mainly attributed to the instability of the Co-Zn compound phase.

4. Discussion

The weight loss behavior of Co-10%W alloy was found to be similar to that of pure cobalt, as seen in Fig. 2. In our previous result,[12)] the rate-controlling step for the pure cobalt-zinc reaction was analyzed as the mutual diffusion process of Co & Zn atoms through the $\beta 1$ compound layer. The $\beta 1$ layer was confirmed to be formed in the Co-10%W alloy, too. Thus, it seems reasonable that the rate-controlling step for the reaction of the Co-10%W alloy with zinc is the same mutual diffusion process through the $\beta 1$ layer. However, the amount of weight loss drastically increased with increasing tungsten content (above 20%) in cobalt (Fig. 2). The compositional analysis seen in Fig. 4 reveals that the $\beta 1$ compound layer could not be formed in the Co-20%W alloy. It was found in the Co-30%W alloy (Fig. 5) that the Co-Zn compound couldn't form a stable layer and only $\gamma 2$ phases were inhomogeneously distributed in the Zinc matrix. The increase of reaction rate in this alloy is understandable considering the instability of the reaction compound.

Fig. 6 shows the cross-sectional optical micrographs of Co-W alloys after reaction with molten zinc at different immersion times. A blooming burst appears in the early stage of reaction (10 min, Fig. 6 (a)) and grows during the next 30 minutes (Fig. 3 (b)). Detailed observation seen in Fig. 6 (a) demonstrates that zinc segregates along the unstable interface in the Co-Zn burst. The formation of the blooming burst in Co-20%W alloy is probably due to the zinc penetration along the grain boundary, especially

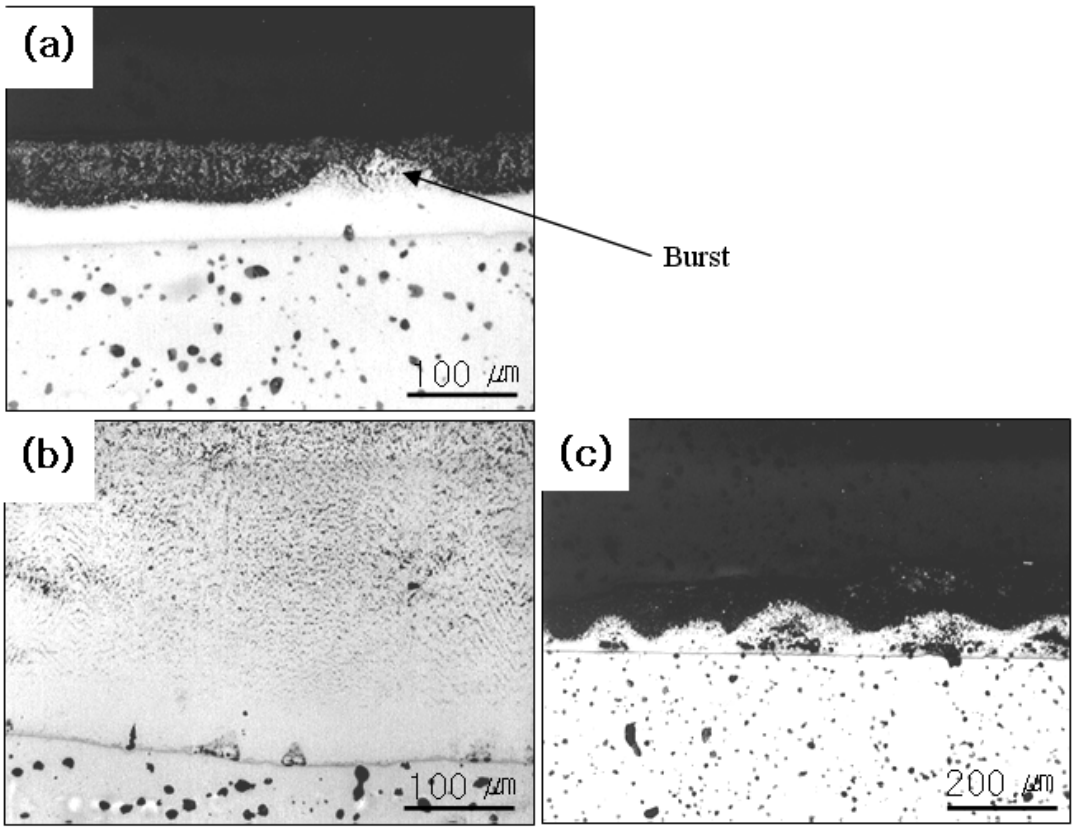

Fig. 6. Cross-sectional optical micrographs of Co-W alloys after reaction with molten pure zinc at 460℃, (a) Co-20%W alloy for 10 min., (b) Co-20%W alloy for 300 min. and (c) Co-30%W alloy for 10 min.

before the complete solution of Co-Zn compound in the molten zinc. As reaction time in molten zinc increases to 5 hours (Fig. 6 (b)), small black zinc particles are found throughout the Co-Zn compound matrix. It is interesting to note that the distribution feature of Zinc particles (Fig. 6 (b)) resembles the wavy characteristic of the tungsten concentrated layer found in the reaction time of 30 minutes (Fig. 4 (b)). Since the tungsten atom has a larger atomic radius, the zinc atom presumably diffuses into the Co-Zn compound along the tungsten concentrated area. Accordingly, zinc penetrates to give rise to the burst blooming in the early stage of reaction and then changes shape and becomes small particles that are distributed throughout the Co-Zn compound matrix with increasing reaction time (Co-20%W alloy).

Fig. 6 (c) shows a typical example of frequent burst on the surface of Co-Zn reaction compound (reaction time of 10 min.) especially observed in the Co-30%W alloy. It is also important to remember when analyzing Fig. 3 and Fig. 5 that the Co-Zn compound in the Co-30%W alloy is difficult to be connected and easily dispersed in the zinc layer. Consequently, a stable Co-Zn layer cannot be formed with increasing tungsten content in cobalt. It is assumed that the grain boundary energy of the Co-Zn compound increases with increasing tungsten content in cobalt and can exceed the interface energy between the Co-Zn compound and molten zinc at a limit value of tungsten. Further study should be performed on the effect of tungsten content on the interface energy of a Co-Zn compound with zinc.

5. Conclusions

In this study, the reaction behavior of the Co-10%W, Co-20%W and Co-30%W alloys in molten zinc was investigated and the reaction mechanism was also discussed. The following conclusions were obtained.

(1) The weight loss behavior of Co-10%W alloy was similar to that of pure cobalt. The relationship between the weight loss and the square root of immersion period represents a straight line in both alloys. As the tungsten content in the Co-W alloy increases, the weight loss behavior fails to follow a linear relationship and the amount weight loss significantly increases.

(2) The Co-Zn reaction layer in Co-10%W alloy was analyzed and found to consist of four intermetallic compounds-- $\gamma 2$, $\gamma 1$, γ and $\beta 1$, similar to the reaction phases in pure cobalt. It was suggested that the mutual diffusion process of Co and Zn through the $\beta 1$ compound layer is the rate-controlling mechanism of these reactions.

(3) In the case of Co-20%W alloy, three kinds of $\gamma 2$, $\gamma 1$ and γ phases were found in the Co-Zn reaction compound without $\beta 1$ phase and a wavy pattern with high tungsten content was also observed. In contrast, only the $\gamma 2$ phase of the Co-Zn compound was found in the Co-30%W alloy as a mixture with zinc in the zinc layer.

(4) Zinc penetration along interface of Co-Zn compound gives rise to blooming burst during the reaction. It was also confirmed that Co-Zn reaction phases became unstable with increasing tungsten content in the Co-W alloy. The increase of reaction rate with increasing W content is mainly due to the instability of the Co-Zn reaction phases.

Acknowledgments

This research was supported by a program for the Training of Graduate Students in Regional Innovation, which was conducted by the Ministry of Commerce Industry and Energy of the Korean Government.

References

1. M. Nakagawa, J. Sakai, T. Ohgouchi, and H. Ohkoshi, *Tetsu to Hagane*, **81**, 989 (1995).
2. M. Sawa, J. Oohori, *Processing of International Thermal Spray Conference '95*, p.37, Kobe, Japan (1995).
3. H. Nakahira, Y. Harada, and K. Tani, *Proc. ATTAC' 88*, p.73, Osaka, Japan (1988).
4. H. Nakahira, Y. Harada, T. Doi, Y. Takatani, and T. Tomita, *J. High Temp. Soc*., **16**, 317 (1990).
5. D. Horstmann, *Proc. 6th Inter. Conf. on H.D.G.*, p.319, London, ZDA (1962).
6. D. Horstmann and F. Peters, *Proc. 9th Inter. Conf. on H.D.G*., p.75, London, ZDA (1971).
7. H. Koga, Y Uchiyama, and T. Aki, *J. Jpn. Inst. Met*., **42**, 136 (1978).
8. T. Tomita, Y. Takatani, Y. Kobayashi, Y. Harada, and H. Nakahira, *ISIJ International*, **33**, 982 (1993).
9. K. Tani, T. Tomita, Y. Kobayashi, Y. Takatani, and Y. Harada, *ISIJ International*, **34**, 822 (1994).
10. B. G. Seong, S. Y. Hwang, M. C. Kim, and K. Y. Kim, *J. Kor. Inst. Met. & Mater.*, **38**, 488 (2000).
11. B. G. Seong, S. Y. Hwang, M. C. Kim, and K. Y. Kim, *Surface and Coatings Technology*, **138**, 101 (2001).
12. B. G. Seong, S. H. Kwon, K. Y. Kim, and K. A. Lee, *TMS 2007*, p.17, Orlando, Florida, USA, Feb. 25 Mar. 2 (2007).
13. A. Hoffman and R. Mohs, *Metall*, **28**, 661 (1974).
14. T. B. Massalski, Binary Alloy Phase Diagrams, 2nd edition, Co-W, ASM Int. (1990).
15. T. B. Massalski, Binary Alloy Phase Diagrams, 2nd edition, Co-Zn, ASM Int. (1990).
16. K. Yajima and T. Yamaguchi, *Powder Metall. International*, **14**, 90 (1982).
17. M. R. Rijnders and F. J. J. van Loo, Scripta Metall.

et Mater., **32**, 1931 (1995).
18. C. Xiaoming, J. Xinchang, and H. Wenxiang, *Proc. of environmental & energy efficient heat treatment tech*., p.250, Beijing, China, Sept. 15-17 (1993).
19. W. Hodge, R. M. Evans, and A. F. Haskins, Trans. AIME, **203**, 824 (1955).